Journal of Nuclear Materials 400 (2010) 251–256

Contents lists available at ScienceDirect

Journal of Nuclear Materials

journal homepage: www.elsevier.com/locate/jnucmat

Spark plasma sintering of iodine-bearing apatite

S. Le Gallet [a,*], L. Campayo [b], E. Courtois [b], S. Hoffmann [c], Yu. Grin [c], F. Bernard [a], F. Bart [b]

[a] Laboratoire Interdisciplinaire Carnot de Bourgogne, UMR 5209 CNRS-UB, 9 Av. Alain Savary, BP 47870, 21078 Dijon Cedex, France
[b] CEA, DEN, Marcoule, DTCD/SECM/LDMC, BP 17171, 30207 Bagnols-sur-Cèze Cedex, France
[c] Max-Planck-Institut für Chemische Physik fester Stoffe, Nöthnitzer Straße 40, 01187 Dresden, Germany

ARTICLE INFO

Article history:
Received 15 December 2009
Accepted 17 March 2010

ABSTRACT

The high chemical durability of iodine-bearing apatite makes it strongly prospective for conditioning of radioactive iodine. The synthesis and consolidation of iodine-bearing compounds require low temperatures to avoid iodine volatilization. Spark plasma sintering therefore appears to be a suitable process because of its shorter treatment time and lower sintering temperature compared with other processes such as HUP or HIP. Two alternatives were examined: SPS sintering of iodine-bearing apatite powder and SPS reacting of a stoichiometric lead iodide and lead phosphovanadate powder mixture. The degree of densification and the microstructure of bulk materials in both cases are described and compared. Reactive sintering appears to involve a three-stage mechanism: (i) PbI_2 coalescence, (ii) solid-state iodoapatite synthesis and consolidation and, (iii) iodoapatite consolidation in the presence of a liquid phase. The SPS reacted products reveal the finest and most homogeneous microstructure, and a density exceeding 96%.

1. Introduction

One of the management strategies examined for long-lived nuclear wastes involves a deep geological disposal. Repository safety is based on conditioning the waste in a chemically inert matrix to ensure radionuclide retention in the event of contact with a dissemination vector. In the case of iodine-129, with a half-life of 15.7 million years, apatite-derivative minerals with the generic formula $Pb_{10}(VO_4)_{6(1-x)}(PO_4)_{6x}I_2$ are promising conditioning materials [1,2]. They are capable of high iodine loading (>8 wt.%) with strong containment properties based on normalized leaching tests [3]. Ceramics with no open porosity are required to limit the potential exchange surface area; this implies the use of materials with a densification exceeding 92% of the theoretical density, a threshold generally acknowledged as marking the elimination of open porosity. However, the densification of iodine-bearing materials requires low sintering temperatures to prevent volatilization; iodoapatite, $Pb_{10}(VO_4)_{4.8}(PO_4)_{1.2}I_2$, decomposes in air above 500 °C. The densification of this type of iodine-bearing apatite was therefore initially envisaged only in a confined environment [3,4]. This can be obtained with an excess of lead phosphovanadate, $Pb_3(VO_4)_{2(1-x)}(PO_4)_{2x}$, which is densified at relatively low temperatures [5,6] and can be consumed as a reagent in the event of PbI_2 diffusion during heating. The balance equation for the formation of iodine-bearing apatite can be written as follows:

$$3Pb_3(VO_4)_{2(1-x)}(PO_4)_{2x} + PbI_2 \rightarrow Pb_{10}(VO_4)_{6(1-x)}(PO_4)_{6x}I_2$$

This work concerns spark plasma sintering (SPS) of iodine-bearing apatite: $Pb_{10}(VO_4)_{4.8}(PO_4)_{1.2}I_2$. Earlier work in a confined environment showed that spark plasma sintering of this phase was possible at temperatures below 500 °C and therefore theoretically without the need for a gangue material [7,8]. Spark plasma sintering of iodoapatite without a gangue was investigated first, then the synthesis and consolidation of this phase by reactive sintering was examined.

2. Experimental procedure

Iodoapatite $Pb_{10}(VO_4)_{4.8}(PO_4)_{1.2}I_2$ was synthesized from lead phosphovanadate $Pb_3(VO_4)_{1.6}(PO_4)_{0.4}$ and lead iodide PbI_2. Iodoapatite is formed with a volume shrinkage by 1.804 cm^3 per mole. This calculation is based on the theoretical reaction written above, taking into account the molar mass for each phase and the following densities: 7.302, 6.099 and 7.117 g cm^{-3} for $Pb_3(VO_4)_{1.6}(PO_4)_{0.4}$, PbI_2 and $Pb_{10}(VO_4)_{4.8}(PO_4)_{1.2}I_2$ respectively.

Lead phosphovanadate was obtained by calcining a powder mixture of PbO (99.3% purity, Prolabo, France), V_2O_5 (99.2% purity, Alfa Aesar, Germany) and $NH_4H_2PO_4$ (97.5% purity, Prolabo, France) for 1 h at 1000 °C at a molar ratio of 3:0.8:0.4. After calcining, the lead phosphovanadate was wet-ground for 240 min in a zirconia bowl (Attritor 01-HD, Union Process). The specific surface area of the product was determined by the BET method (Gemini 2360, Micrometrics) to be 7.0 m^2 g^{-1}. A few traces of hydroxyapatite $Pb_{10}(VO_4)_6(OH)_2$ were identified, most likely arising from a

* Corresponding author. Tel.: +33 380396163; fax: +33 380396167.
E-mail address: sophie.le-gallet@u-bourgogne.fr (S. Le Gallet).

0022-3115/$ - see front matter © 2010 Elsevier B.V. All rights reserved.
doi:10.1016/j.jnucmat.2010.03.011

dissolution–reprecipitation reaction during oven-drying of the powder. DSC analysis (Netzsch STA 409) in argon (heating rate 10 °C min^{-1}) showed that the lead phosphovanadate is stable up to its melting point at 960 °C.

Lead iodide was obtained by precipitation of an acidic lead nitrate solution (pH(25 °C) = 5) with a stoichiometric amount of a sodium iodide solution (molar ratio Pb:I = 1:2). The filtered precipitate was rinsed in denatured ethanol and dried at 80 °C. Characterization of the product by X-ray diffraction (XRD, Siemens D5000, $\lambda_{Cu\beta}$ = 1.3924 Å) revealed no traces of crystalline impurities. The lead iodide powder synthesized for this study did not notably include lead hydroxyiodide PbIOH, an impurity generally found in commercial lead iodide. Thermal decomposition of the latter releases water and iodine which are unfavorable to densification, and leads to the formation of lead oxyiodides. DSC analysis of the prepared PbI_2 (Netzsch DSC 204) in argon (heating rate 10 °C min^{-1}) revealed two endothermic peaks at 307 °C and 374 °C. The first can be attributed to the decomposition of lead carbonate traces. IR analysis (Bruker Vertex 70 spectrometer) of the PbI_2 powder showed a low-intensity 1390 cm^{-1} band characteristic of the carbonate group; this impurity was present either as amorphous or in trace amounts and, thus, did not appear on the XRD diagram. It may be formed during the synthesis by precipitation and/or after the synthesis by contact with air. The second endothermic peak may correspond to the formation of a eutectic involving PbI_2 and PbO resulting from the decomposition of $PbCO_3$ [9].

The reagent mixture of lead phosphovanadate $Pb_3(VO_4)_{1.6}(PO_4)_{0.4}$ and lead iodide PbI_2 was obtained by co-milling of ground lead phosphovanadate and lead iodide powders for 240 min in ethanol in a zirconia bowl. The specific surface area of 9.5 m^2 g^{-1} for the reagent mixture was determined by the BET method. SEM observation (Zeiss Supra 55) showed that it consisted of poorly cohesive agglomerates containing fine particles as well as micrometric platelets, smaller than 10 μm (Fig. 1a). EDXS analysis identified the fine particles as a mixture of $Pb_3(VO_4)_{1.6}(PO_4)_{0.4}$ and PbI_2, and the platelets as PbI_2. DSC analysis of the reagent mixture showed a broad exothermic signal between 250 °C and 390 °C, suggesting a start of the reaction. XRD characterization of the mixture revealed traces of hydroxyvanadinite arising from the lead phosphovanadate. The XRD diagram was interpreted from the Langford method [10] in order to estimate the size of the crystallites in the reagent mixture: 17 nm for $Pb_3(VO_4)_{1.6}(PO_4)_{0.4}$. The size of the PbI_2 crystallites could not be estimated by this method, as some of the crystallites (platelets) were too large.

Iodoapatite was obtained by calcining stoichiometric quantities of lead iodide and lead phosphovanadate for 15 h at 720 °C in a sealed quartz ampoule. The iodoapatite powder was then ground under the same conditions as the reagent mixture. Its specific surface area was 5.8 m^2 g^{-1}, and it consisted of strongly cohesive agglomerates of nanometric particles (<100 nm, Fig. 1b). XRD characterization revealed also a secondary minor phase, PbV_6O_{11}. The size of 14 nm for the iodoapatite crystallites was estimated from XRD patterns by the Langford method [10].

The iodoapatite powder and reagent powder mixture of $Pb_3(VO_4)_{1.6}(PO_4)_{0.4}$ and PbI_2 (1.675 g for each experiment) were SPS treated in graphite molds (inner diameter = 10 mm) by spark plasma sintering (SPS 515S, Syntex Inc.) at temperatures below 500 °C. At these conditions, iodoapatite does not decompose with iodine release. The effects of temperature, dwell time and pressure on the microstructure were investigated at the constant heating rate of 50 °C min^{-1} in order to keep constant the effect of the temperature overshoot by SPS processing. The powder was first compacted at room temperature under a pressure of 70 MPa. The green density of iodoapatite and of the reagent mixture was 69.8% and 60%, respectively. This discrepancy can be attributed to the difference in the specific surface area of the two powders, and to the non-spherical shape of the PbI_2 platelets in the reagent mixture. Tests are summarized in Table 1.

The density of all the samples was determined by hydrostatic weighing using Archimedes method. The samples were examined by scanning electron microscopy (Zeiss Supra 55) after fracture, as the microstructure was very difficult to discern after chemical etching. We also verified by X-ray diffraction that the $Pb_{10}(VO_4)_{4.8}(PO_4)_{1.2}I_2$ phase was conserved during the non-reactive SPS sintering and that it was formed in the case of SPS reactive sintering. The theoretical density of this compound determined by XRD is 7.117 g cm^{-3} [1] and, the relative density of the ceramics indicated below corresponds to the ratio between the hydrostatic density and the theoretical one. If the reaction is incomplete, the relative density is slightly underestimated, since the density of the mixture is only 7.102 g cm^{-3}. When the reaction was not complete, the mass fractions of the iodoapatite formed and the precursors that did not react were determined (±5%) in the samples by XRD analysis (a piece of the sample was ground). A calibration curve was established for this purpose with a mixture of iodoapatite with increasing quantities of reactants (lead phosphovanadate and lead iodide) from the $I^*_{(1\,1\,1)}/I^*_{(1\,1\,1)} + I^*_{(1\,1\,0)}$ ratio, where $I^*_{(1\,1\,1)}$ and $I^*_{(1\,1\,0)}$ are the areas of the (1 1 1) and (1 1 0) peaks on XRD diagrams for iodoapatite and lead phosphovanadate respectively.

3. Results

3.1. Reactive versus non-reactive sintering

No pressure rise was observed in the chamber during sintering, regardless of the conditions, indicating that no iodine volatilization

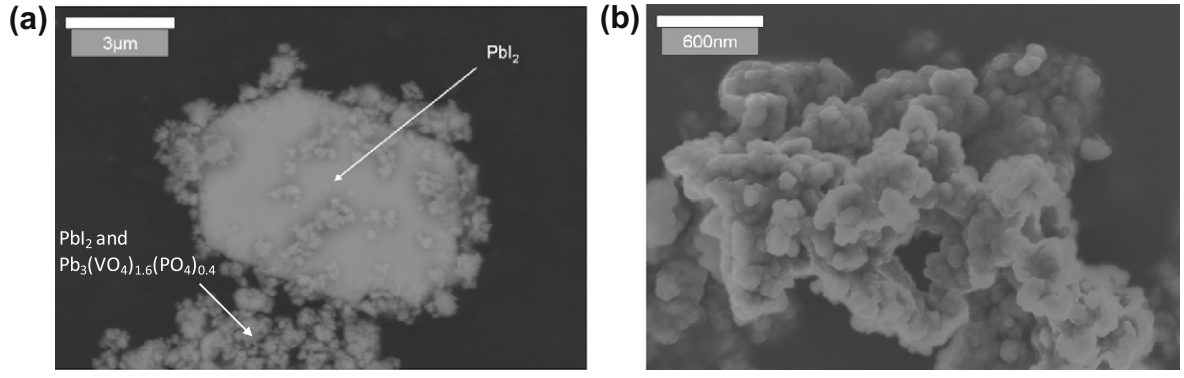

Fig. 1. SEM images of powder samples: (a) reagent mixture after attrition; (b) iodoapatite after thermal treatment at 720 °C in quartz ampoule and attrition.

Table 1
Relative density and grain size for different SPS treatment conditions.

Test designation	Dwell temperature (°C)	Dwell time (min)	Pressure (MPa)	Relative density (%)	Grain size (nm)	Crystallite size (nm)
Non-reactive sintering						
IAp-001	400	20	40	81.6 ± 0.1	Abnormally large	51 ± 3
IAp-002	400	20	70	88.1 ± 0.4	Abnormally large	52 ± 3
IAp-003	450	20	40	88.4 ± 0.5	Abnormally large	63 ± 3
IAp-004	450	20	70	91.8 ± 0.1	Abnormally large	33 ± 2
Reactive sintering						
PbI2-001	400	5	40	97.2 ± 0.5	138 ± 42	40 ± 2
PbI2-002	400	20	40	96.9 ± 0.5	145 ± 44	57 ± 3
PbI2-003	400	5	70	97.1 ± 0.4	148 ± 38	24 ± 1
PbI2-004	450	5	40	96.9 ± 0.5	167 ± 45	39 ± 2

occurred during these tests. XRD analysis showed that the $Pb_{10}(VO_4)_{4.8}(PO_4)_{1.2}I_2$ phase was conserved during SPS sintering and, that the reactants were completely converted to iodoapatite in the case of SPS reacting. The iodoapatite crystallites were systematically larger in the case of non-reactive sintering, except for sample IAp-001 (51 nm) compared with the sample PbI2-002 (57 nm) produced under the same conditions (Table 1).

Pore closure was not obtained by non-reactive sintering (Table 1). Moreover, the microstructure of these samples was not homogeneous. A porosity gradient could be observed within the ceramic between the denser periphery and the lower-density core (Fig. 2a). In addition, the size of some grains exceeded ten micrometers and exhibited abnormal growth (Fig. 2b); they coexisted with submicronic grains arising from normal growth. In contrary, the samples obtained by SPS reacting were of uniform density and grain size (Fig. 2c and d). While the samples PbI2-001 to PbI2-004 revealed single-phase microstructures, the IAp samples contained a small fraction of a vanadium-rich secondary phase, the lead vanadium oxide PbV_6O_{11}, which appears with dark contrast in the BSE images (Fig. 3). This phase was initially present in the iodoapatite powder. However, its composition determined by a semi-quantitative EDXS analysis deviates slightly from the stoichiometric value with a lead excess (36.8 instead of 30.1 wt.%) and a deficit of vanadium (39.2 instead of 44.4 wt.%).

In the case of non-reactive SPS sintering, as expected, the temperature and pressure were favorable to densification (Table 1).

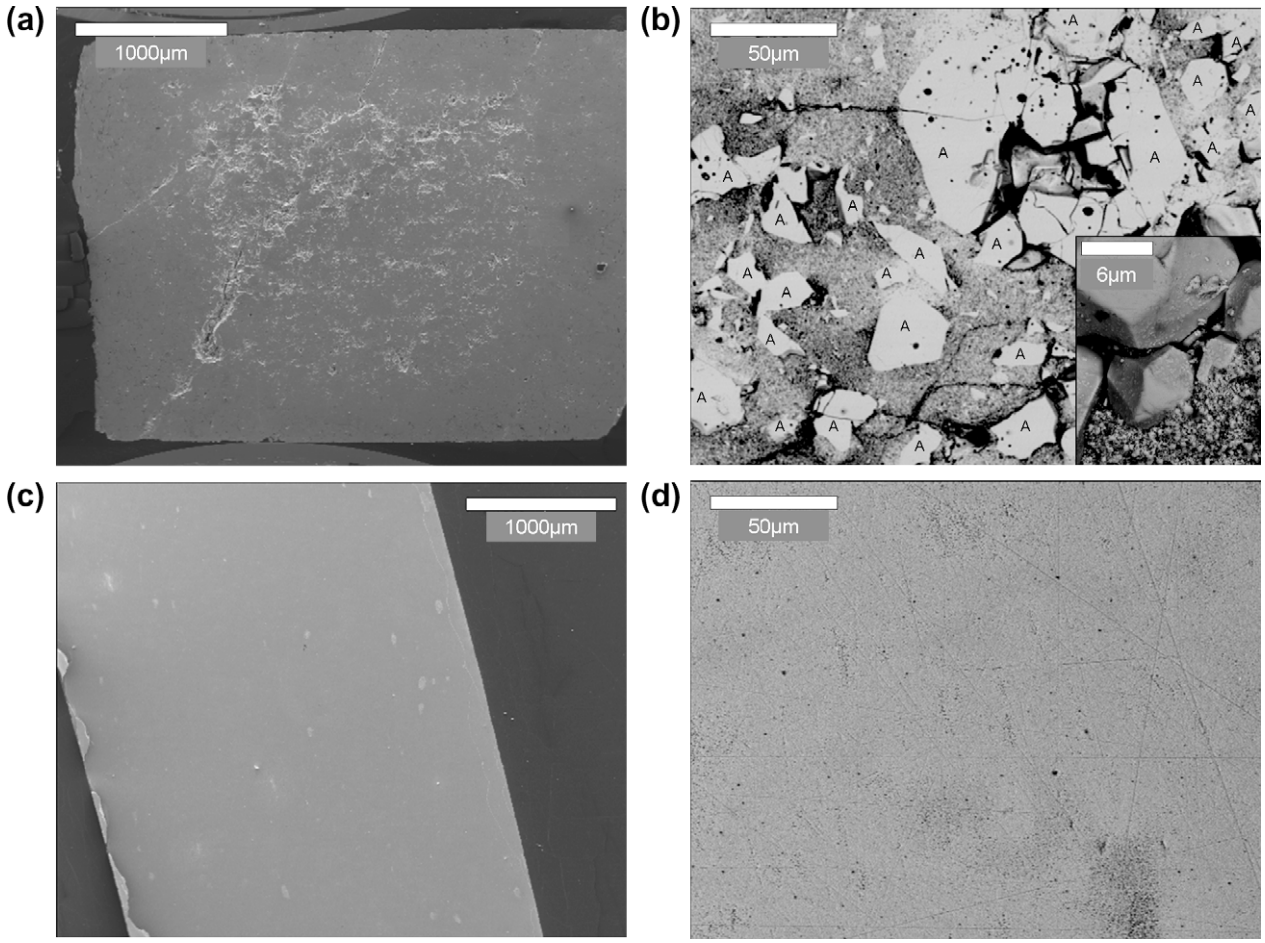

Fig. 2. Microstructure of the SPS sintered and SPS reacted samples: (a) porosity gradient in the sample IAp-001 (400 °C, 20′, 40 MPa); (b) abnormal growth in the sample IAp-001 (400 °C, 20′, 40 MPa). Some grains which exhibit an abnormal growth were labeled on Fig. 2b by the ≪A≫ capital letter; (c) uniform microstructure of the sample PbI2-001 (400 °C, 5′, 40 MPa); (d) absence of abnormal growth traces in the microstructure of the sample PbI2-001 (400 °C, 5′, 40 MPa).

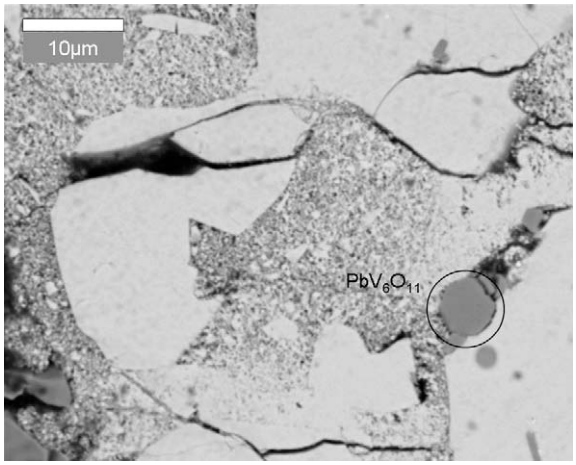

Fig. 3. Backscatter-electron image of sample IAp-002 (400 °C, 20′, 70 MPa): large light grey grains represent the target iodoapatite (abnormal growth), the dark grains (circle) reveal the secondary phase PbV_6O_{11}.

Moreover, the elevated pressure allowed the dwell temperature to be reduced by 50 °C (Fig. 4): for the same density, a sintering at 400 °C under 70 MPa is equivalent to a sintering at 450 °C under 40 MPa. Sample characterization also showed a change in the microstructure depending on the processing conditions. The density gradient between the core and periphery diminished when the treatment temperature and/or pressure increased (samples IAp-002, IAp-003 and IAp-004). This gradient is commonly observed in SPS sintered ceramics and, is attributable to sample heating by the mold and not by Joule effect due to a current flow in the sample [11–13]. An increase of the dwell temperature and/or pressure favors an abnormal particle growth.

In the case of reactive sintering, no effects of temperature, dwell time or pressure were observed on the densification, probably because a high relative density had already been reached at lower temperature, time and pressure (Table 1). All "PbI2" samples were of uniform density and show similar grain size (Table 1). The grain size was chosen as equal to the mean value of grain size measurements of about 200 grains (five photos were randomly taken by SEM on a fractured surface of each sample). This is consistent with the shrinkage curves shown in Fig. 4 where, after densification, samples PbI2-001, PbI2-002 and PbI2-004 all form a single curve bundle. However, an increase of the pressure from 40 MPa to 70 MPa shifts the beginning of the shrinkage temperature by 150 °C. In this case, the sintering pressure is equal to the compacting pressure.

The shrinkage doubled between sintering of the iodoapatite powder and the reagent mixture, although the difference in the relative density did not exceed 15% (Fig. 4). This is caused by the higher green density of iodoapatite compared with the reagent mixture. Despite the higher green density of iodoapatite, the small increase in density during sintering did not result in shrinkage of the same magnitude as for the reagent mixture. Two hypotheses can be postulated to account for this difference in sintering behavior: the most obvious is the powder grain size, and the second possibility is a difference in the sintering mechanism. The powder fineness was not in this case responsible for the improved sinterability, since a coarser reagent mixture ($3.3\ m^2\ g^{-1}$) was better densified than the iodoapatite powder. We therefore decided to investigate the sintering mechanism involved in reactive sintering.

3.2. Understanding reactive sintering

The shrinkage curves for iodoapatite and for the reagent mixture suggest very different behavior during sintering. The shrinkage derivative (versus temperature) of the iodoapatite has a single minimum (at 395 °C under 40 MPa and at 375 °C under 70 MPa). The situation is more complex in the case of SPS reacting with a very low initial shrinkage rate that increases strongly above 350 °C. The shrinkage curves for SPS reacting show two changes of slope, regardless of the pressure applied. For this reason, SPS reacting experiments were performed by stopping the treatment without the dwell at 225, 300 and 375 °C under 40 MPa and 70 MPa to aid in interpreting the reaction mechanism. The relative densities and XRD data for these six samples are shown in Table 2 and in Fig. 5 respectively.

Table 2
Operating conditions and relative density of SPS reacted samples without dwell time.

Test designation	Dwell temperature (°C)	Pressure (MPa)	Relative density (%)
PbI2-005	225	40	61.5 ± 0.3
PbI2-006	225	70	65.8 ± 0.3
PbI2-007	300	40	66.5 ± 0.4
PbI2-008	300	70	72.3 ± 0.6
PbI2-009	375	40	81.1 ± 0.1
PbI2-010	375	70	91.3 ± 0.5

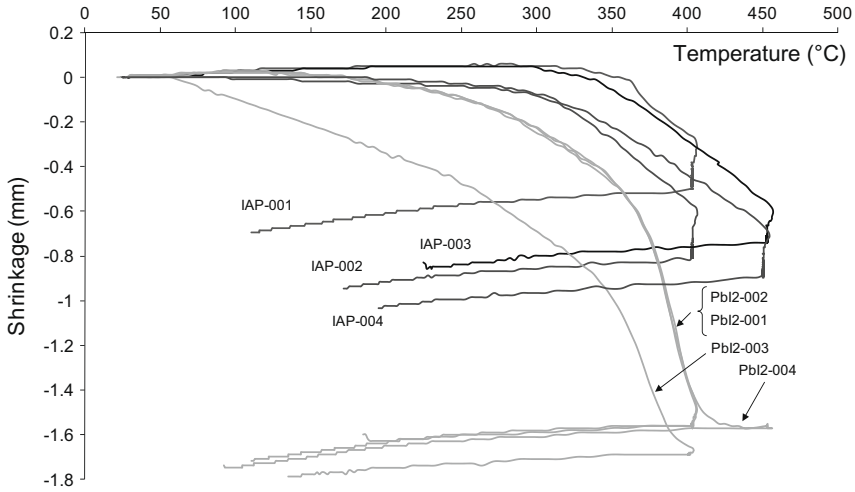

Fig. 4. Shrinkage curves for SPS sintered (IAp-001 to IAp-004) and SPS reacted samples (PbI2-001 to PbI2-004) in dependence of treatment conditions.

Iodoapatite appears to form at 300 °C regardless of the pressure applied. Under 40 MPa the sample contained 33 wt.% iodoapatite compared with 37 wt.% under a pressure of 70 MPa. At 225 °C its presence was suspected in the sample sintered at 70 MPa, but could not be definitely determined by XRD as the reagent mixture contained hydroxyapatite, which hinders identification of iodoapatite. Thermogravimetric analysis of hydroxyapatite showed that it does not decompose at 225 °C. At 375 °C, the precursors were still found: quantitative XRD analysis showed that samples PbI2-010 and PbI2-009 still contained 19 wt.% of precursors. Traces of hydroxyapatite in the reactant mixture induce an error on the amount of lead phosphovanadate available to form iodoapatite. From a thermogravimetric analysis of the powder, the real mass of lead phosphovanadate was calculated. The error made on this value, when the mixture is prepared, leads to a variation of 3.6 wt.% in the formation of iodoapatite. However, this error is lower than the precision given by the XRD quantification.

Regardless of the processing conditions, the sample microstructure was heterogeneous (according to SEM). Stacks of platelets less than 100 nm thick and frequently more than 20 μm long were systematically observed next to strongly spheroidal grains. EDXS analysis of the platelets showed that they were formed by lead iodide. As an illustration, Fig. 6 shows the microstructure of sample PbI2-006 (225 °C, 40 MPa). It is in agreement with morphology of the initial powder (Fig. 1a). However, these platelets were significantly larger than those present initially in the reagent mixture. They were oriented preferentially within the sample with the stacking direction parallel to the applied pressure vector $\vec{\mathbf{F}}$ (Fig. 6, right). The preferential orientation of PbI_2 platelets in the samples is also verified in the XRD patterns. Indeed, the intensity ratio is not in agreement with the theoretical data. The peak (0 0 1) of this phase, supposed to be to 25%, is in fact the most intense. During the first step of the shrinkage, the relative density of the samples differed only slightly from the green density (at 225 °C, 61.5% and 65.8% for 40 MPa and 70 MPa respectively). It therefore appears that,

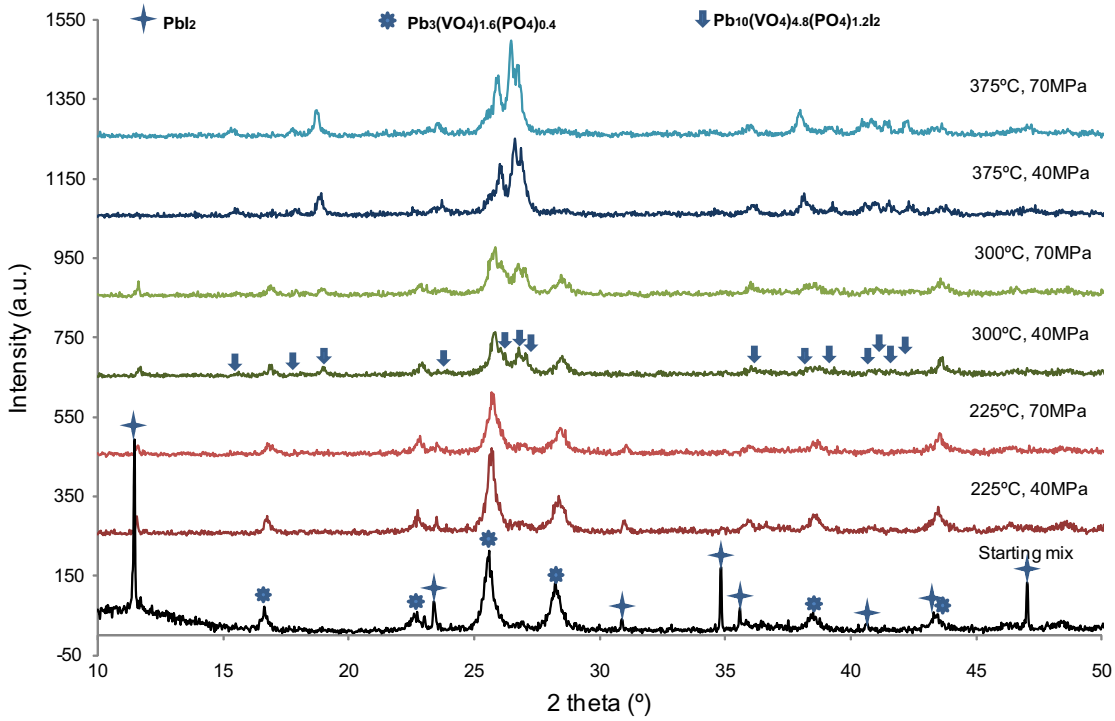

Fig. 5. XRD patterns of samples obtained by SPS reacting experiments without dwell time.

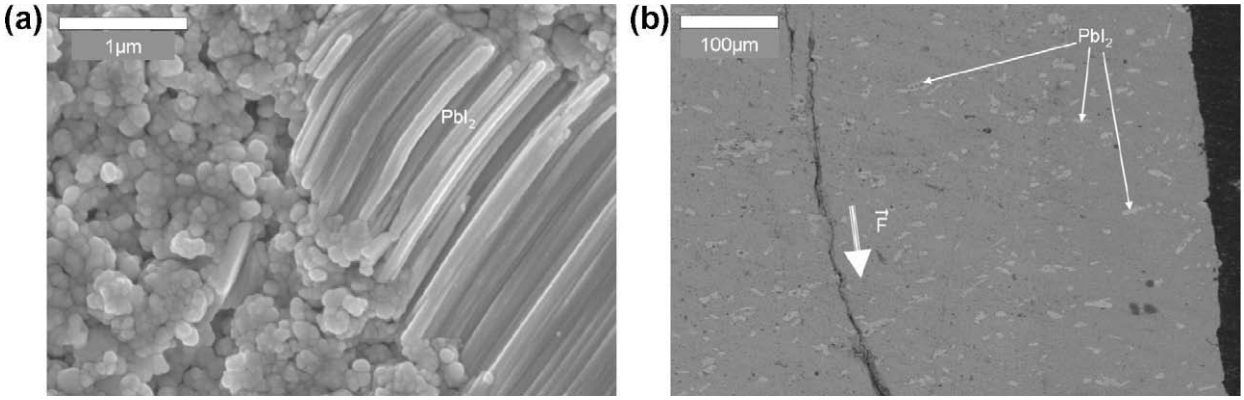

Fig. 6. SEM images of the sample PbI2-006: (a) after fracture; (b) polished cross section.

whatever the pressure, macroscopic shrinkage of the sample below 250 °C can be attributed to the coalescence of lead iodide in the form of platelets whose surface normal is parallel to the direction of load application. The coalescence phenomenon seems to be more important under 70 MPa.

During the second step of the shrinkage, iodoapatite synthesis occurred. Iodoapatite synthesis takes place between 250 °C and 390 °C and naturally results in strong shrinkage. However, the shrinkage here observed for this temperature range is too large to be due to iodoapatite synthesis alone. Complete conversion of the precursors to iodoapatite results in a 1.01 mm^3 volume reduction for 1.675 g of reactant mixture. The volume reduction is based on the volume shrinkage (1.804 cm^3 per mole) calculated for the iodoapatite formation. In the case of a sample 10 mm in diameter, this represents a thickness variation of 0.01 mm. Consequently, iodoapatite densification happens during its synthesis (solid-phase sintering) and both continue during a part of the third step of the shrinkage between 350 °C and 400 °C at 70 MPa (or between 370 °C and 430 °C at 40 MPa) when trace amounts of precursors are present. Lead iodide is indeed less reactive being in the form of micrometric platelets due to the low contact surface with the lead phosphovanadate particles, and was still present at 375 °C. The shrinkage rate in this temperature range is higher than for iodoapatite powder, confirming that the densification mechanism is not the same. The presence of residual lead iodide between 350 °C and 400 °C at 70 MPa and between 370 °C and 430 °C at 40 MPa could account for the densification mechanism observed in the case of SPS reacting. Lead iodide melts at 380 °C. Moreover, at 374 °C it forms a eutectic with PbO (an impurity generated by the decomposition of carbonate traces in lead iodide) [9]. The liquid phase generated in the material would thus result in liquid-phase sintering, increasing the densification rate. However, no traces of such a phase were found in grain boundaries on SEM images of the samples. The molten PbI_2, injected under the pressure effect through the interconnected network, may have disappeared by reaction with residual lead phosphovanadate. On the contrary, the molten PbI_2, originally found as large platelets, in "tanks", is not entirely converted during the SPS reacting experiments at 375 °C and re-crystallizes during the cooling phase. This results in porosity around the re-crystallized PbI_2 grains (Fig. 7). This morphology of "ghosts" was only found for SPS reacting experiments carried out at 375 °C where the beginning of the melting of PbI_2 or the eutectic reaction with PbO was likely to happen. The increase of the temperature and dwell time (PbI2-001 to PbI2-004) allows to convert the molten PbI_2 even in "tanks". The transition temperature between solid-phase sintering and liquid-phase sintering appears to depend on the mechanical pressure applied (370 °C at 40 MPa versus 350 °C at 70 MPa). Nonetheless, the samples also exhibited different microstructures as a function of the mechanical pressure. Indeed, the thickness of the remaining PbI_2 particles at temperatures 370 °C or 350 °C were 80 nm at 40 MPa and 30 nm at 70 MPa. It has been shown that in the case of gold particles, a reduction in diameter from 25 to 5 nm reduces the observed melting temperature of gold from 1336 K to 300 K [14]. However, no data are available in the literature supporting the hypothesis that this dimensional variation of thickness of PbI_2 platelets would lower the temperature of the PbO–PbI_2 eutectic or the melting temperature of PbI_2.

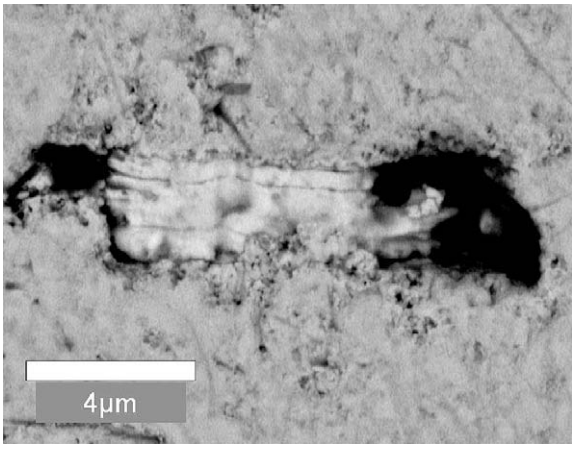

Fig. 7. SEM image of the sample PbI2-009 (polished cross section).

4. Conclusion

Non-reactive sintering of iodine-bearing apatite $Pb_{10}(VO_4)_{4.8}(PO_4)_{1.2}I_2$ by spark plasma sintering results in about 91% densification in the temperature range between 400 °C and 450 °C. Densification is limited mainly by abnormal particle growth. At lower temperatures and pressures a density gradient appears between the pellet periphery and core. This gradient reflects the temperature gradient in the material during sintering. In the case of SPS reacting, samples with homogeneous composition and density were obtained; their relative density exceeds 96% in every case. The higher efficiency of SPS reacting for the densification level can be attributed to the accelerated mass transfer during the reaction, in particular by the molten PbI_2. Spark plasma reacting is thus an interesting alternative to other sintering processes for pelletizing iodine-bearing apatite.

Acknowledgement

The authors would like to thank the GNR 3051 Matinex for funding this research.

References

[1] F. Audubert, Mise au point d'une matrice apatitique pour le confinement de l'iode 129. PhD thesis, Institut National Polytechnique de Toulouse, 1995.
[2] J. Carpena, F. Audubert, J.L. Lacout, Procédé de conditionnement d'iode radioactif, en particulier d'iode 129, utilisant une apatite comme matrice de confinement, Patent n° 9414706 (07/12/94), WO 1996/181266 A1 (13/07/96).
[3] C. Guy, F. Audubert, J.E. Lartigue, C. Latrille, T. Advocat, C. Fillet, CR. Phys. 3 (1–8) (2002) 827–837.
[4] E.R. Maddrell, P.K. Abraitis, Mater. Res. Soc. Symp. Proc. 807 (2004) 261–266.
[5] T. Robin, D. Bernache-Assollant, F. Audubert, Powder Technol. 103 (1) (1999) 10–18.
[6] T. Robin, D. Bernache-Assollant, F. Audubert, J. Eur. Ceram. Soc. 20 (9) (2000) 1231–1240.
[7] L. Campayo, S. Le Gallet, Yu. Grin, E. Courtois, F. Bernard, F. Bart, J. Eur. Ceram. Soc. 29 (8) (2009) 1477–1484.
[8] L. Campayo, S. Le Gallet, F. Bart, F. Bernard, Yu. Grin, Utilisation de la technique de frittage Flash pour la synthèse et la densification d'iodoapatite, Patent n° 0758128 (08/10/07), WO 2009/047246 A1 (16/04/09).
[9] W. Rolls, E.A. Secco, U.V. Varadaraju, Mater. Sci. Eng. 65 (1984) L5–L8.
[10] J.L. Langford, The determination of microstructural properties by means of pattern decomposition, in: E. Prince, J.K. Stalick (Eds.), Accuracy in Powder Diffraction II, Gaitherburg, MD, USA, 1992, pp. 110–126 (NIST special publication).
[11] K. Matsugi, H. Kuramoto, T. Hatayama, O. Yanagisawa, J. Mater. Process. Technol. 146 (2004) 274–281.
[12] U. Anselmi-Tamburini, S. Gennari, J.E. Garay, Z.A. Munir, Mater. Sci. Eng. A394 (2005) 139–148.
[13] K. Vanmeensel, A. Laptev, J. Hennicke, J. Vleugels, O. Van der Biest, Acta Mater. 53 (2005) 4379–4388.
[14] Ph. Buffat, J.-P. Borel, Phys. Rev. A 13 (6) (1976) 2287–2298.